

Turbulent magnetic decay controlled by two conserved quantities

Axel Brandenburg^{1,2,3,4,†} and Aikya Banerjee⁵

¹Nordita, KTH Royal Institute of Technology and Stockholm University, Hannes Alfvéns väg 12, SE-10691 Stockholm, Sweden

²The Oskar Klein Centre, Department of Astronomy, Stockholm University, AlbaNova, SE-10691 Stockholm, Sweden

³McWilliams Center for Cosmology & Department of Physics, Carnegie Mellon University, Pittsburgh, PA 15213, USA

⁴School of Natural Sciences and Medicine, Ilia State University, 3–5 Cholokashvili Avenue, 0194 Tbilisi, Georgia

⁵Department of Physical Sciences, Indian Institute of Science Education and Research Kolkata, Mohanpur 741246, West Bengal, India

(Received 18 June 2024; revised 2 November 2024; accepted 4 November 2024)

The decay of a turbulent magnetic field is slower with helicity than without. Furthermore, the magnetic correlation length grows faster for a helical than a non-helical field. Both helical and non-helical decay laws involve conserved quantities: the mean magnetic helicity density and the Hosking integral. Using direct numerical simulations in a triply periodic domain, we show quantitatively that in the fractionally helical case the mean magnetic energy density and correlation length are approximately given by the maximum of the values for the purely helical and purely non-helical cases. The time of switchover from one to the other decay law can be obtained on dimensional grounds and is approximately given by $I_H^{1/2} I_M^{-3/2}$, where I_H is the Hosking integral and I_M is the mean magnetic helicity density. An earlier approach based on the decay time is found to agree with our new result and suggests that the Hosking integral exceeds naive estimates by the square of the same resistivity-dependent factor by which also the turbulent decay time exceeds the Alfvén time. In the presence of an applied magnetic field, the mean magnetic helicity density is known to be not conserved, and we show that then also the Hosking integral is not conserved.

Keywords: astrophysical plasmas, plasma simulation

1. Introduction

In recent years, there has been significant interest in the study of decaying turbulent magnetic fields. One of the main applications has been to the understanding of the magnetic field evolution during the radiation-dominated era of the early universe

† Email address for correspondence: brandenb@nordita.org

(Brandenburg, Enqvist & Olesen 1996; Christensson, Hindmarsh & Brandenburg 2001; Banerjee & Jedamzik 2004). The special case with finite magnetic helicity has been studied and understood for a long time (Hatori 1984; Biskamp & Müller 1999). It is the prime example of large-scale magnetic field growth due to an inverse cascade. The possibility of such an inverse cascade is explained by the conservation of magnetic helicity (Frisch *et al.* 1975). However, even in the absence of magnetic helicity, an inverse cascade can develop (Kahniashvili *et al.* 2013; Zrake 2014; Brandenburg, Kahniashvili & Tevzadze 2015), and it is well explained by the conservation of what is now called the Hosking integral (Hosking & Schekochihin 2021, 2023a; Zhou, Sharma & Brandenburg 2022; Brandenburg, Sharma & Vachaspati 2023c), which is the correlation integral of the magnetic helicity density.

In all the cases mentioned above, either the magnetic helicity density was vanishing, so the spectral magnetic helicity was zero at all wavenumbers and the decay governed by the conservation of the Hosking integral, or the magnetic helicity density was finite and the spectral magnetic helicity had the same sign at all wavenumbers, so the decay was governed by the conservation of the mean magnetic helicity density. A special situation was studied in the work of Brandenburg, Kamada & Schober (2023b), where the magnetic helicity was finite, but it was balanced by fermion chirality of the opposite sign so that the net chirality was vanishing. For such a system, the decay was again successfully explained by the conservation of the Hosking integral, which was adapted to include the chirality from the fermions.

We have seen that the Hosking integral can be applied to broad ranges of systems where magnetic helicity is still important locally, but globally the net magnetic helicity vanishes. However, there is an important class of astrophysically relevant systems, where the magnetic field is not generated by magnetogenesis, as in the early universe, but by dynamo action. This means that some of the kinetic energy of turbulent motions is converted into magnetic energy. It is important to stress that, even if the velocity field were helical, i.e. if there is finite kinetic helicity in the system, as is generally the case when there is rotation and stratification of density and/or velocity, magnetic helicity conservation still precludes the generation of magnetic helicity, at least on dynamical time scales (Ji 1999).

In the aforementioned helically driven large-scale dynamos, magnetic helicity can be generated at small scales, but it is then balanced by magnetic helicity at large scales so as to conserve magnetic helicity. Alternatively, we can also say that magnetic helicity is produced at large scales, for example by the tilting of buoyantly rising magnetic flux tubes in cyclonic convective events, as envisaged by Parker (1955). Magnetic helicity conservation then implies magnetic twist of opposite sign at smaller scales. In practice, because there is always finite magnetic diffusivity, which acts especially on small scales, the magnetic helicity from large scales will, after some time, dominate the total magnetic helicity owing to the loss at small scales where the magnetic helicity has the opposite sign. Therefore, there is always a small imbalance between the contributions from small and large length scales. It is therefore a situation that is only partially suited to the phenomenology involving the conservation of the Hosking integral.

If we now were to turn off the driving, the turbulence would gradually decay. This decay should then be governed by the conservation of both the Hosking integral and the mean magnetic helicity density. Both helical and non-helical cases lead to inverse cascading, where the magnetic field decays more slowly than the velocity field, leading ultimately to a magnetically dominated state. Such conditions could apply to the decay of a magnetic field produced in a proto-neutron star. There, we expect a turbulent dynamo to occur that is driven by convection (Thompson & Duncan 1993). This would happen when the neutrino

opacity is large enough to prevent neutrinos from escaping freely (Epstein 1979; Burrows & Lattimer 1986).

Another source of turbulence in proto-neutron stars could be the magnetorotational instability that results from the radially outward decreasing angular velocity gradient associated with collapsed material having an approximately constant angular momentum density (Guilet *et al.* 2022). In both cases, the turbulence itself has kinetic helicity of opposite signs in the northern and southern hemispheres (negative in the north and positive in the south). In each hemisphere, this leads to dynamo action of the type described above, but the magnetic helicities have opposite signs not only in the two hemispheres, but also on small and large length scales. One would thus focus only on one hemisphere and ignore the interaction between north and south. The magnetic helicities from small and large length scales would then nearly cancel. Such fields have been called ‘bihelical’ and their decay properties were first studied by Yousef & Brandenburg (2003). They found that the positive and negative contributions rapidly mix and annihilate, and that the ratio of the magnetic helicity spectrum to the magnetic energy spectrum has local extrema at both small and large scales, although the latter is dominant in an absolute sense.

Since the net magnetic helicity of a bihelical magnetic field does not vanish exactly, and since the mean magnetic helicity itself is an important conserved quantity, we are confronted with a situation where the magnetic decay is governed by two conserved quantities. Investigating this aspect in a more controlled fashion is the main purpose of this paper.

In an earlier paper, Tevzadze *et al.* (2012) studied a case with fractional helicity. They found that the correlation length developed a steeper growth (indicative of magnetic helicity domination) at a specific moment that depends on the value of the magnetic helicity as well as on the initial values of the magnetic energy and the magnetic correlation length. This consideration provided a quantitative estimate for the time of the switchover from non-helical to helical scalings. A similar estimate was provided by Hosking & Schekochihin (2021) based on the scaling of the Hosking integral I_H . One may then ask whether the time of the switchover from a decay controlled by I_H to that controlled by the mean magnetic helicity density I_M can be computed based on dimensional arguments. Indeed, given that the quantity I_H has dimensions $\text{cm}^9 \text{s}^{-4}$ and I_M has dimensions $\text{cm}^3 \text{s}^{-2}$ (see Brandenburg (2023), and note that the magnetic field is here understood to be in Alfvén units with dimensions cm s^{-1}) a combination of I_H and I_M that yields a time would be $I_H^{1/2} I_M^{-3/2}$. It will turn out that this is indeed the time of switchover between the two regimes.

2. Our model

2.1. Basic equations

We simulate the compressible magnetohydrodynamic equations with an isothermal equation of state with constant sound speed c_s , so the pressure p and the density ρ are related by $p = \rho c_s^2$. The equations for the magnetic vector potential \mathbf{A} , the velocity \mathbf{U} and the logarithmic density $\ln \rho$ are

$$\frac{\partial \mathbf{A}}{\partial t} = \mathbf{U} \times \mathbf{B} + \eta \nabla^2 \mathbf{A}, \quad (2.1)$$

$$\frac{D\mathbf{U}}{Dt} = -c_s^2 \nabla \ln \rho + \frac{1}{\rho} [\mathbf{J} \times \mathbf{B} + \nabla \cdot (2\rho \nu \mathbf{S})], \quad (2.2)$$

$$\frac{D \ln \rho}{Dt} = -\nabla \cdot \mathbf{U}, \quad (2.3)$$

where $D/Dt = \partial/\partial t + \mathbf{U} \cdot \nabla$ is the advective derivative, $\mathbf{B} = \nabla \times \mathbf{A}$ is the magnetic field, $\mathbf{J} = \nabla \times \mathbf{B}/\mu_0$ is the current density, μ_0 is the vacuum permeability, ν is the viscosity and $S_{ij} = (\partial_i U_j + \partial_j U_i)/2 - \delta_{ij} \nabla \cdot \mathbf{U}/3$ are the components of the traceless rate-of-strain tensor \mathbf{S} . Our computational domain is a periodic cube of size L^3 , and $k_1 = 2\pi/L$ is the smallest wavenumber. Since the mass in the domain does not change, the volume-averaged density is constant in time, i.e. $\langle \rho \rangle = \text{const.} \equiv \rho_0$. Here and below, angle brackets denote volume averaging.

2.2. Initial conditions

In our idealized studies, we focus on the decay governed by two conserved quantities (Hosking integral and mean magnetic helicity density). We construct an initial magnetic vector potential in Fourier space as $\tilde{\mathbf{A}}(\mathbf{k}) = \mathbf{R}(\mathbf{k}; \zeta) \tilde{\mathbf{A}}^{\text{nhel}}$, where

$$R_{ij}(\mathbf{k}; \zeta) = \delta_{ij} - \hat{k}_i \hat{k}_j + i \hat{k}_\ell \zeta \epsilon_{ij\ell} \quad (2.4)$$

is a matrix with \hat{k}_i being the components of the unit vector $\hat{\mathbf{k}} = \mathbf{k}/k$, $|\zeta| \leq 1$ is a non-dimensional parameter that quantifies the fractional helicity and $\tilde{\mathbf{A}}^{\text{nhel}}$ is a non-helical field with random phases and possesses the desired spectrum for the magnetic field $\text{Sp}(\mathbf{B}) = k^2 \text{Sp}(\mathbf{A})$, i.e.

$$\text{Sp}(\mathbf{B}) = \frac{A_0 k^\alpha}{1 + (k/k_0)^{5/3+\alpha}}, \quad (2.5)$$

where A_0 is an amplitude, k_0 denotes the initial position of the spectral peak, α is the subinertial range slope (here always $\alpha = 4$) and the inertial range has a $k^{-5/3}$ spectrum. Note that \mathbf{A} is by construction periodic. Therefore, $\mathbf{B} = \nabla \times \mathbf{A}$ has zero mean field. At the end of this paper, we also briefly discuss a case with a finite mean magnetic field.

The strength of the magnetic field can be characterized by the Alfvén speed, $v_A = B_{\text{rms}}/\sqrt{\mu_0 \rho_0}$, which is here based on the mean density. For $\zeta \neq 0$, we have a finite magnetic helicity and expect then the decay to be governed by both the Hosking integral and the mean magnetic helicity density.

In (2.5), $\text{Sp}(\cdot)$ denotes a shell integrated spectrum. This operation will also be applied to the local, gauge-dependent magnetic helicity density $h = \mathbf{A} \cdot \mathbf{B}$, so that $\text{Sp}(h) = (k^2/8\pi^3 L^3) \int_{4\pi} |\tilde{h}|^2 d\Omega_k$. The tilde marks a quantity in Fourier space, and Ω_k is the solid angle in Fourier space, so that $\int \text{Sp}(h) dk = \langle h^2 \rangle$, and likewise for $\int \text{Sp}(\mathbf{B}) dk = \langle \mathbf{B}^2 \rangle$. Owing to the integration over shells in three-dimensional wavenumber space, the spectrum of a spatially random (δ correlated) field is proportional to k^2 . This is indeed the case for a globally non-helical field, where $\langle h \rangle = 0$.

2.3. Definitions of the Hosking integral

The Hosking integral \mathcal{I}_H is defined as the asymptotic limit of the magnetic helicity density correlation integral:

$$\mathcal{I}_H(R) = \int_{V_R} \langle h(\mathbf{x}) h(\mathbf{x} + \mathbf{r}) \rangle d^3 r, \quad (2.6)$$

for scales R large compared with the correlation length ξ_M of the turbulence, but small compared with the system size L . Here, $V_R = 4\pi R^3/3$ is the volume of a sphere of radius R . For small values of R , the function $\mathcal{I}_H(R)$ increases proportional to R^3 , but for large R , it levels off when there is no net magnetic helicity. However, as explained in Hosking & Schekochihin (2021), this is different for finite magnetic helicity, as is discussed below. In

Run	k_0/k_1	ζ	v_{A0}/c_s	v_{Am}/c_s	Ma	Lu	$I_M/2\xi_M\mathcal{E}_M$	N^3	Figures
A	60	1	0.57	0	0.20 \rightarrow 0.03	1000 \rightarrow 2500	0.95 \rightarrow 0.94	1152 ³	1
B	30	0.003	0.21	0	0.10 \rightarrow 0.005	2700 \rightarrow 1500	0.01 \rightarrow 0.13	1024 ³	2, 3, 8
C	60	0.01	0.20	0	0.10 \rightarrow 0.001	1300 \rightarrow 800	0.06 \rightarrow 0.78	1024 ³	4–8
D	60	0	0.22	0.1	0.11 \rightarrow 0.001	800 \rightarrow 70	0	1024 ³	9

TABLE 1. Summary of runs presented in this paper. The arrows indicate the change from the beginning to the end of the run.

practice, the value of R is chosen empirically and must always be small compared with the size of the domain.

Zhou *et al.* (2022) devised and compared different methods for computing $\mathcal{I}_H(R)$. These methods are all based on the Fourier transform of h . Particularly simple is what they called the box-counting method for a spherical volume with radius R . This allowed them to rewrite (2.6) as a weighted integral over $\text{Sp}(h)$:

$$\mathcal{I}_H(R) = \int_0^\infty w(k, R) \text{Sp}(h) dk, \tag{2.7}$$

where

$$w(k, R) = \frac{4\pi R^3}{3} \left[\frac{6j_1(kR)}{kR} \right]^2, \tag{2.8}$$

and $j_1(x) = (\sin x - x \cos x)/x^2$ is a spherical Bessel function.

2.4. Input and diagnostic parameters of the model

Important input parameters of the model are the ratio of the initial Alfvén speed to the sound speed, v_{A0}/c_s . In the presence of an imposed mean field, $\mathbf{B}_m = B_m \hat{\mathbf{x}}$, a case discussed at the end of the paper, the corresponding Alfvén speed is denoted by v_{Am} . To obtain information about the turbulent decay that is independent of the size and shape of the computational domain, we must choose the value of k_0/k_1 to be sufficiently large. However, it should also not be chosen too large, because it would diminish the range of wavenumbers between k_0 and the largest wavenumber in the domain, which is called the Nyquist wavenumber, $k_{Ny} = k_1 N/2$, where N is the number of mesh points. The sensitivity of the results on the choice of k_0 has been studied on various occasions (e.g. Zhou *et al.* 2022). A reasonable compromise that still allows for sufficiently large Reynolds numbers seems to be $k_0/k_1 = 60$. This is the value that is used for the main run in the present paper, but we also present some results with $k_0/k_1 = 30$; see table 1 for a summary of runs presented in this paper.

To characterize the degree of compressibility and the vigour of turbulence, we quote the Mach and Lundquist numbers:

$$Ma = u_{\text{rms}}/c_s, \quad Lu = v_A/\eta k_0. \tag{2.9a,b}$$

Since our model is spatially homogeneous, it can be characterized by the magnetic energy and helicity spectra, $E_M(k, t)$ and $H_M(k, t)$, respectively. They are normalized such that

their integrals give the mean magnetic energy and helicity densities, $\mathcal{E}_M \equiv \int E_M(k, t) dk = \langle \mathbf{B}^2 \rangle / 2\mu_0$ and $I_M \equiv \int H_M(k, t) dk = \langle \mathbf{A} \cdot \mathbf{B} \rangle$, respectively.¹

The position of the peak of the spectrum is characterized by the inverse magnetic integral scale, $k_{\text{peak}} = \xi_M^{-1}$, where ξ_M is here defined as

$$\xi_M = \int k^{-1} E_M(k, t) dk \bigg/ \int E_M(k, t) dk. \quad (2.10)$$

Of particular importance are the time dependencies $\xi_M(t)$ and $\mathcal{E}_M(t)$, which, in turn, are characterized by the instantaneous scaling exponents $q(t) = d \ln \xi_M / d \ln t$ and $p(t) = -d \ln \mathcal{E}_M / d \ln t$. The relative magnetic helicity can be computed as the non-dimensional ratio $I_M / 2\xi_M \mathcal{E}_M$, which is between -1 and $+1$.

The relevant information that quantifies the Hosking integral is the first non-vanishing coefficient in the Taylor expansion:

$$\text{Sp}(h)|_{k \rightarrow 0} = \frac{I_H}{2\pi^2} k^2 + \dots; \quad (2.11)$$

see Hosking & Schekochihin (2021), Schekochihin (2022) and Zhou *et al.* (2022) for details. This is also the primary method used here to determine the value of I_H ; see Zhou *et al.* (2022) for a comparison between different methods. We confirm that $2\pi^2 \text{Sp}(h) / k^2$ has an approximately flat part for small values of k and use its value at $k = k_1$ to measure I_H . Below, we also confirm that I_H is nearly independent of time; see Zhou *et al.* (2022) for quantitative assessment of its invariance in the ideal limit. Note that, since $\int \text{Sp}(h) dk = \langle h^2 \rangle$, which has dimensions $(\text{cm}^3 \text{ s}^{-2})^2$, $\text{Sp}(h)$ has dimensions $\text{cm}^7 \text{ s}^{-4}$ and therefore I_H has dimensions $\text{cm}^9 \text{ s}^{-4}$, as expected.

To facilitate comparison with other work, it is useful to present our results in non-dimensional form. The time used in the numerical simulations is made non-dimensional by plotting the evolution versus $c_s k_1 t$, which is convenient for numerical reasons, because c_s and k_1 are constant in time. However, physically more meaningful would be a non-dimensionalization by using the Alfvén speed and the inverse correlation length. Both are time dependent, but the values v_{Ae} and k_e at the end of the simulations seem to be most meaningful.

2.5. Run time and scale separation

To obtain meaningful results, two important constraints need to be obeyed. First, the value of Lu needs to be large enough so that we are in the regime of developed turbulence. Second, the subinertial range must always be large enough so that, by the end of the run, its slope is not affected by finite size effects of the computational domain. This automatically limits the maximum run time below which our results can still be meaningful. Both constraints can only be obeyed in the limit of infinite resolution. In practice, the largest resolution that is presently feasible is typically 2048^3 mesh points (Zhou *et al.* 2022), but this large resolution does already constrain the number of experiments that can reasonably be performed. Therefore, we use for most of our simulations a lower resolution of $N^3 = 1024^3$ mesh points. In that case, the largest wavenumber in the domain is $k_{\text{Ny}} = k_1 N / 2 = 512 k_1$. As discussed above, this led us to the compromise of choosing the values 30 and 60 for the scale separation ratio k_0 / k_1 , so $k_0 / k_{\text{Ny}} = 17-8.5$, leaving barely enough dynamical range for turbulence to develop.

¹The name I_M has been chosen here to mark its important role as an ideal invariant and to highlight its usage analogously to that of the Hosking integral I_H .

i	β	q	p	σ	$C_i^{(\xi)}$	$C_i^{(\mathcal{E})}$	$C_i^{(E)}$
M	0	2/3	2/3	1/3	0.13	4.1	0.7
H	3/2	4/9	10/9	1/9	0.12	3.7	0.025

TABLE 2. Summary of the coefficients characterizing the decays governed by the conservation of magnetic helicity ($i = M$) and the Hosking integral ($i = H$).

3. Results

In the present context, we have to deal with two conserved quantities, namely the Hosking integral I_H and the mean magnetic helicity density $I_M = \langle \mathbf{A} \cdot \mathbf{B} \rangle$. The former case has been studied extensively in recent years. Specifically, Brandenburg & Larsson (2023) and Brandenburg *et al.* (2023c) found

$$\xi_M(t) \approx 0.12 I_H^{1/9} t^{4/9}, \quad \mathcal{E}_M(t) \approx 3.7 I_H^{2/9} t^{-10/9}, \quad E_M(k, t) \lesssim 0.025 I_H^{1/2} (k/k_0)^{3/2}. \tag{3.1a-c}$$

The hope is that the coefficients in these expressions are universal, but it should be noted that they have not yet been verified in other contexts.

3.1. Decay controlled by mean and fluctuating magnetic helicities

In the helical case with $I_M \neq 0$, we have $\xi_M \propto t^{2/3}$ and $\mathcal{E}_M \propto t^{-2/3}$ (Hatori 1984; Biskamp & Müller 1999; Brandenburg & Kahniashvili 2017). In the present context, the pre-factors are important. Using the data from figures 1(c) and 2(c) of Brandenburg & Kahniashvili (2017), here referred to as Run A, we find

$$\xi_M(t) \approx 0.12 I_M^{1/3} t^{2/3}, \quad \mathcal{E}_M(t) \approx 4.3 I_M^{2/3} t^{-2/3}, \quad E_M(k, t) \lesssim 0.7 I_M. \tag{3.2a-c}$$

Generally, we can write

$$\xi_M(t) = C_i^{(\xi)} I_i^\sigma t^q, \quad \mathcal{E}_M(t) = C_i^{(\mathcal{E})} I_i^{2\sigma} t^{-p}, \quad E_M(k) = C_i^{(E)} I_i^{(3+\beta)\sigma} (k/k_0)^\beta, \tag{3.3a-c}$$

where the index i in the integrals I_i and the coefficients $C_i^{(\xi)}$, $C_i^{(\mathcal{E})}$ and $C_i^{(E)}$ stands for M or H for magnetic helicity and Hosking scalings, respectively, and σ is the exponent with which length enters in I_i : $\sigma = 1/3$ for the magnetic helicity density ($i = M$) and $\sigma = 1/9$ for the Hosking integral ($i = H$); see table 2 for a summary of the coefficients.²

In figure 1, we show the magnetic energy spectra, as well as compensated evolutions of $\xi_M(t)$ and $\mathcal{E}_M(t)$ for the maximally helical run (Run A). We see that the peak of $\mathcal{E}_M(t)$ remains underneath a nearly flat envelope (its slope is $\beta = 0$), as is expected for a fully helical turbulent decay at late times. The compensated evolutions of $\xi_M(t)$ and $\mathcal{E}_M(t)$ are not yet fully converged towards the end of that run (the lines are not yet flat). This is partially caused by the insufficient scale separation between the box wavenumber k_1 and that of the spectral peak by the end of the run. Nevertheless, we can read off the approximate values $C_M^{(\xi)} \approx 0.12$ and $C_M^{(\mathcal{E})} \approx 4.3$ towards the end of the run. The values of these coefficients are revisited later in this paper.

²In (3.3c), we have here corrected a typo in (12c) of Brandenburg & Larsson (2023) and (3.1c) of Brandenburg *et al.* (2023c), where the exponent on I_i was incorrectly stated as $(3 + \beta)/\sigma$ instead of $(3 + \beta)\sigma$, but the calculations were done correctly.

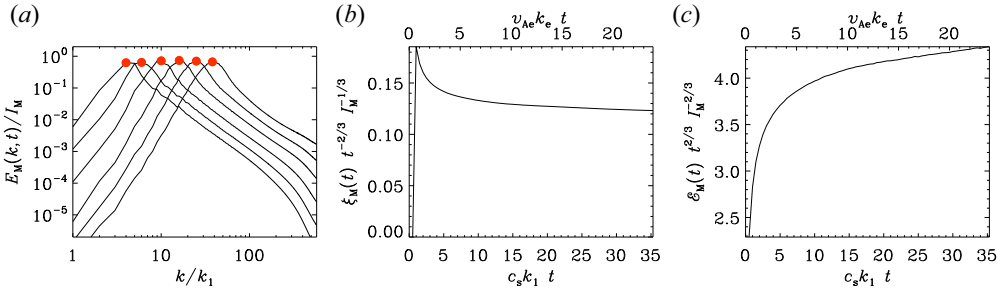


FIGURE 1. (a) Magnetic energy spectra, as well as compensated evolutions of (b) $\xi_M(t)$ and (c) $\mathcal{E}_M(t)$ for the maximally helical run of figure 2(c) of Brandenburg & Kahniashvili (2017), here referred to as Run A. In (a), the red symbols denote the spectral peaks.

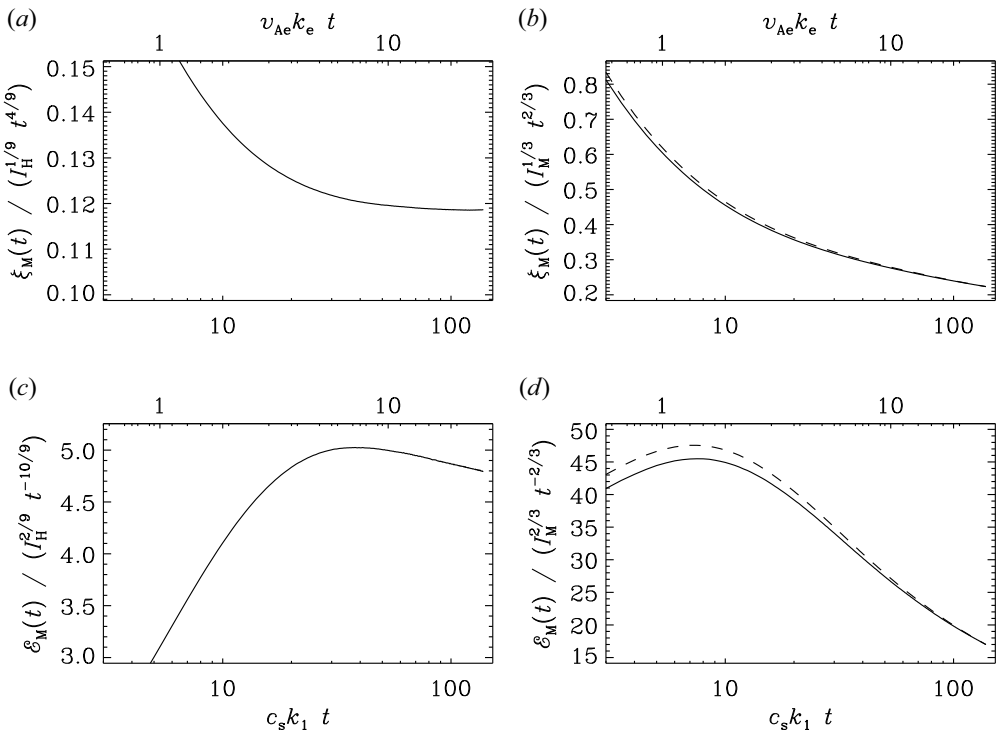


FIGURE 2. Evolution of $\xi_M(t)$ (a,b) and $\mathcal{E}_M(t)$ (c,d) for Run B with $k_0/k_1 = 30$ and $\zeta = 0.003$, compensated by the expected evolution if the decay is controlled either by I_H (a,c) or by I_M (b,d). The dashed line denotes the use of I_M at the end of the run, while for the solid line, the time-dependent value was taken.

In figure 2, we again show the compensated evolutions of $\xi_M(t)$ and $\mathcal{E}_M(t)$, but now for Run B, which is nearly perfectly non-helical ($\zeta = 0.003$) and has $k_0/k_1 = 30$. The resulting coefficients are close to those estimated previously, namely $C_H^{(\xi)} \approx 0.12$ and $C_H^{(\mathcal{E})} \approx 4.7$. This supports the previous hypotheses of Brandenburg & Larsson (2023) and Brandenburg *et al.* (2023c) that these coefficients may indeed be universal.

To determine the value of $I_H(t)$, we plot in figure 3 the evolutions of $(2\pi^2/k^2) \text{Sp}(h)$ (normalized by v_{Ae}^4/k_e^5) for $k/k_1 = 1, 2$ and 3 for Run B. We see that for $k/k_1 = 1$, the

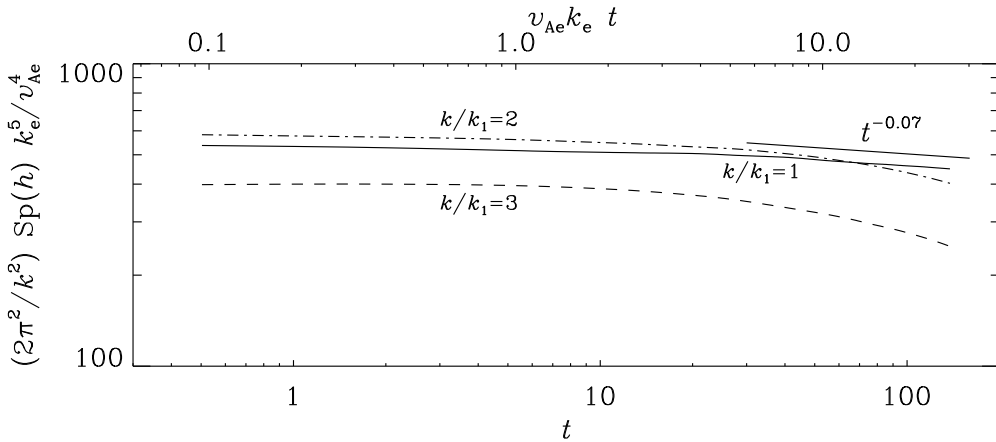


FIGURE 3. Evolutions of $(2\pi^2/k^2) \text{Sp}(h)$, normalized by v_{Ae}^4/k_e^5 , for $k/k_1 = 1$ (solid line), 2 (dashed-dotted line) and 3 (dashed line), for the nearly non-helical Run B with $\zeta = 0.003$ and $k_0/k_1 = 30$.

result shows a nearly negligible decline proportional to $t^{-0.07}$. Note that, in units of v_{Ae}^4/k_e^5 , the value of I_H is about 500.

3.2. Decay controlled by I_M and I_H

If both I_M and I_H control the decay, we have a combination of the two decay laws such that the late times are always controlled by the more strongly conserved quantity, i.e. by I_M . One might expect that the resulting expression for the combination of the decay laws (3.1a–c) and (3.1a–c) is given by the sum of both expressions. This would be analogous to the way how in radiation transport the cooling time is given by the sum of the cooling times for the optically thick and thin cases; see (7) of Brandenburg & Das (2020). In the present case, this would translate to

$$\xi_M \approx 0.12 I_M^{1/3} t^{2/3} + 0.12 I_H^{1/9} t^{4/9}, \tag{3.4}$$

$$\mathcal{E}_M \approx 4.3 I_M^{2/3} t^{-2/3} + 3.7 I_H^{2/9} t^{-10/9}. \tag{3.5}$$

Since the second terms involving I_H are initially larger, but their contributions to ξ_M grow more slowly and that to \mathcal{E}_M decay faster than the first terms, one expects their contributions to become subdominant after some time. Thus, the magnetic helicity will always survive and be the dominant contribution to explaining the decay.

To examine now a run where the decay is controlled by both I_M and I_H , we now increase the initial fractional helicity slightly from 0.003 to 0.01; see figure 4 for magnetic energy spectra at different times for Run C. Note that the peaks of the spectra evolve at first underneath an envelope with the slope $\beta = 3/2$, as expected for a decay controlled by I_H . At later times, however, the envelope becomes flat (slope $\beta = 0$), as expected for a decay controlled by I_M .

In figure 5, we show the evolutions of $\xi_M(t)$ and $\mathcal{E}_M(t)$ for Run C, compensated by $t^{-2/3}$ and $t^{2/3}$, respectively, as well as $t^{-4/9}$ and $t^{10/9}$, respectively. We see that now the curves compensated by $t^{-2/3}$ and $t^{2/3}$, respectively, become nearly constant, as expected for a decay that is governed by magnetic helicity conservation. Specifically, we find $\xi_M/(I_M^{1/3} t^{2/3}) \approx 0.14$ and $\mathcal{E}_M/(I_M^{2/3} t^{-2/3}) \approx 4.0$. During a short intermediate interval,

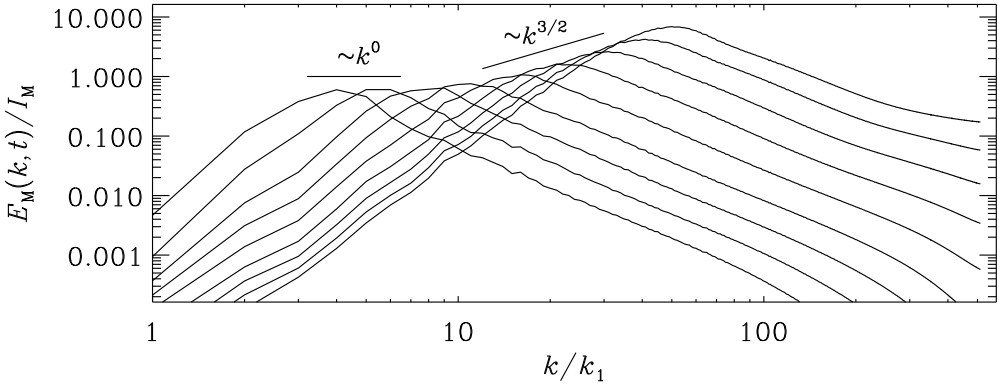


FIGURE 4. Magnetic energy spectra for Run C with $k_0/k_1 = 60$ and $\zeta = 0.01$ at times $v_{Ae}k_e t = 0.07, 0.18, 0.40, 0.82, 1.65, 3.3, 6.1, 11.1$ and 20.7 .

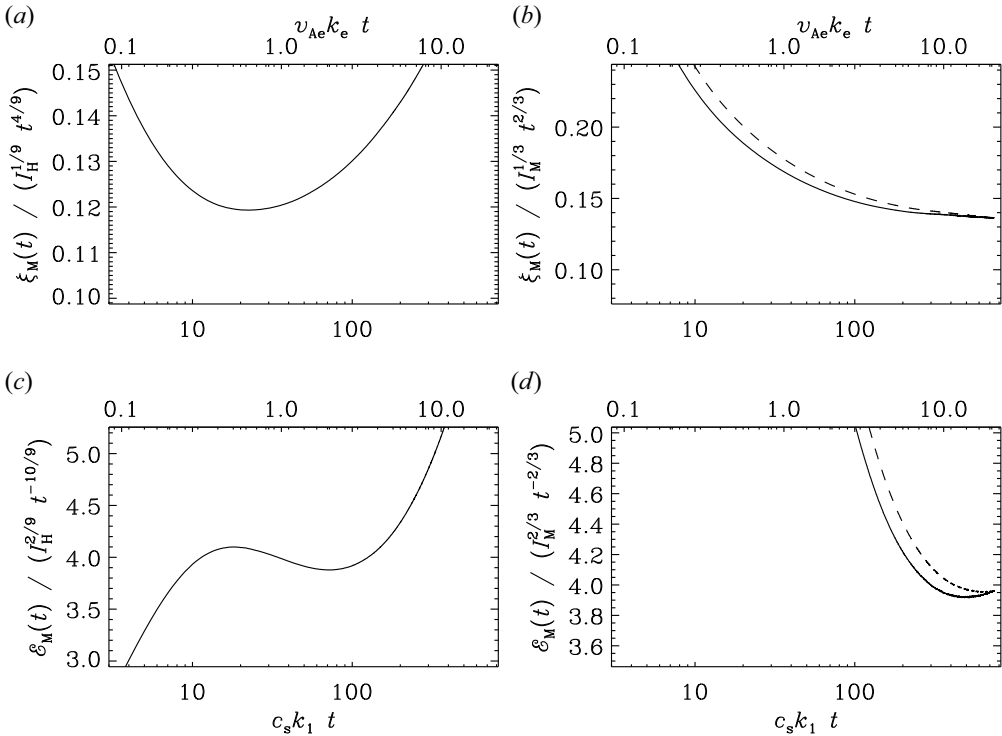


FIGURE 5. Similar to figure 2, but for Run C with $k_0/k_1 = 60$ and $\zeta = 0.01$.

however, we see that the curves compensated by $t^{-4/9}$ and $t^{10/9}$, respectively, show brief plateaus around $v_{Ae}k_e t = 1$ with $\xi_M / (I_H^{1/9} t^{4/9}) \approx 0.12$ and $\mathcal{E}_M / (I_H^{2/9} t^{-10/9}) \approx 4.0$.

3.3. Improved fits with I_M and I_H

We have seen that the limiting cases where the decay is controlled either by I_M or by I_H are well reproduced by (3.1a–c). It turns out, however, that the combined fits given by (3.4) and (3.5) are not very accurate. Improved fits can be obtained by using large weighting

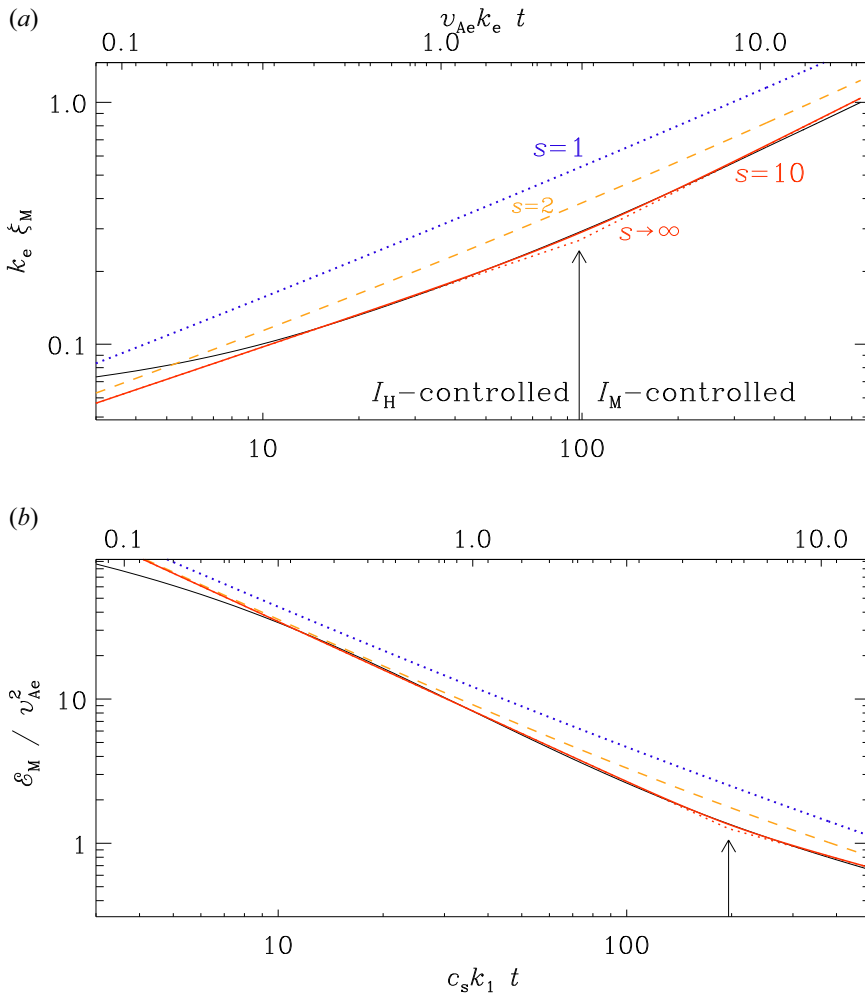


FIGURE 6. Decay of magnetic energy (black line) and the fit given by (3.5) (dotted blue line, denoted by $s = 1$) as well as (3.7) with $s = 2$ (dashed orange line) and $s = 10$ (solid red line). The dotted red line corresponds to the limit $s \rightarrow \infty$, as realized by (3.8) and (3.9).

exponents for both contributions, i.e.

$$\xi_M \approx \left[\left(0.12 I_M^{1/3} t^{2/3} \right)^s + \left(0.14 I_H^{1/9} t^{4/9} \right)^s \right]^{1/s}, \tag{3.6}$$

$$\mathcal{E}_M \approx \left[\left(4.0 I_M^{2/3} t^{-2/3} \right)^s + \left(4.0 I_H^{2/9} t^{-10/9} \right)^s \right]^{1/s}. \tag{3.7}$$

The result is shown in figure 6 for Run C, where we show that $s = 10$ yields satisfactory fits, while $s = 2$ and $s = 1$ (our original hypothesis) are poor. The fact that the coefficients for both parts are different from those of the individual fits and that they happen to be 4.0 in (3.7), but different from each other in (3.6), is probably just by chance and reflect that degree of uncertainty of these values.

It is important to emphasize that the limit $s \rightarrow \infty$ corresponds to

$$\xi_M \approx \max \left(0.12 I_M^{1/3} t^{2/3}, 0.14 I_H^{1/9} t^{4/9} \right), \quad (3.8)$$

$$\mathcal{E}_M \approx \max \left(4.0 I_M^{2/3} t^{-2/3}, 4.0 I_H^{2/9} t^{-10/9} \right). \quad (3.9)$$

These expressions yield discontinuities in the derivative. An advantage of such expressions is that one can clearly see the regimes of validity of both expressions. The critical times when characterizing the crossover from Hosking scaling to magnetic helicity scaling are given by

$$t_\xi \approx (0.12/0.14)^{9/2} (I_H/I_M^3)^{1/2} \approx 0.50 I_H^{1/2} I_M^{-3/2}, \quad (3.10)$$

$$t_\mathcal{E} \approx I_H^{1/2} I_M^{-3/2}. \quad (3.11)$$

It would be plausible to assume that both times should equal each other. The fact that they are not equal to each other might hint, again, at the possibility that the precise values of these coefficients are still uncertain. On the other hand, looking at [figure 5](#), it is actually true that ξ_M approaches the I_M -dominated scaling by a factor two earlier than \mathcal{E}_M . A possible explanation for this behaviour could lie in the fact that the spectral shapes change as the system becomes fully helical. We return to this in [§ 3.4](#), where we discuss the spectral shapes in more detail.

We recall that an essential assumption in our dimensional argument was the fact that the magnetic field is understood to be in Alfvén units and thus has dimensions of cm s^{-1} . In neutron star crusts, by contrast, where the magnetic field is governed by the Hall effect ([Goldreich & Reisenegger 1992](#)), it has units of $\text{cm}^2 \text{s}^{-1}$, so $[I_M] = \text{cm}^5 \text{s}^{-2}$ and $[I_H] = \text{cm}^{13} \text{s}^{-4}$ ([Brandenburg 2023](#)), so t_ξ and $t_\mathcal{E}$ are now proportional to $I_H^{5/6} I_M^{-13/6}$, so both exponents are larger than in the ordinary magnetohydrodynamic case; cf. [\(3.10\)](#) and [\(3.11\)](#). An example of the corresponding switch between the two regimes was presented in [figure 10\(b\)](#) of [Brandenburg \(2020\)](#).

3.4. Collapsed spectra

The quality of the fits of [\(3.6\)](#) and [\(3.7\)](#) for $s = 1$ and $s \rightarrow \infty$ can be examined further by computing compensated spectra. This is shown in [figure 7](#), where the abscissa is scaled with $\xi_M(t)$ and the ordinate with $[\mathcal{E}_M(t)\xi_M(t)]^{-1}$. We see that the collapse in [figure 7\(b\)](#), where $s \rightarrow \infty$, is much better than that in [figure 7\(a\)](#), where $s = 1$, and it is almost as good as that in [figure 7\(c\)](#), where the actual values of $\xi_M(t)$ and $\mathcal{E}_M(t)$ are used. This supports our finding that in the fractionally helical case, the magnetic energy and correlation length are approximately given by the maximum of the values for the purely helical and purely non-helical cases, and not by their sum, as might naively have been expected.

As alluded to in [§ 3.3](#), there is a change in the shape of the spectrum as the system becomes fully helical. In particular, the position of the peak appears for slightly larger values of $k\xi_M(t)$ at later times; see [figure 7\(c\)](#). Thus, the value of $\xi_M(t)$ is slightly overestimated, which would explain the smaller value of t_ξ compared with $t_\mathcal{E}$.

3.5. Comparison with earlier work

As mentioned in the introduction, the switchover time from non-helically to helically dominated decay has been studied by [Tevzadze et al. \(2012\)](#) under the assumption that $p = 1$ and $q = 1/2$ ([Christensson et al. 2001](#)) instead of $p = 10/9$ and $q = 4/9$, as now motivated by the conservation of the Hosking integral. The basic idea is to assume

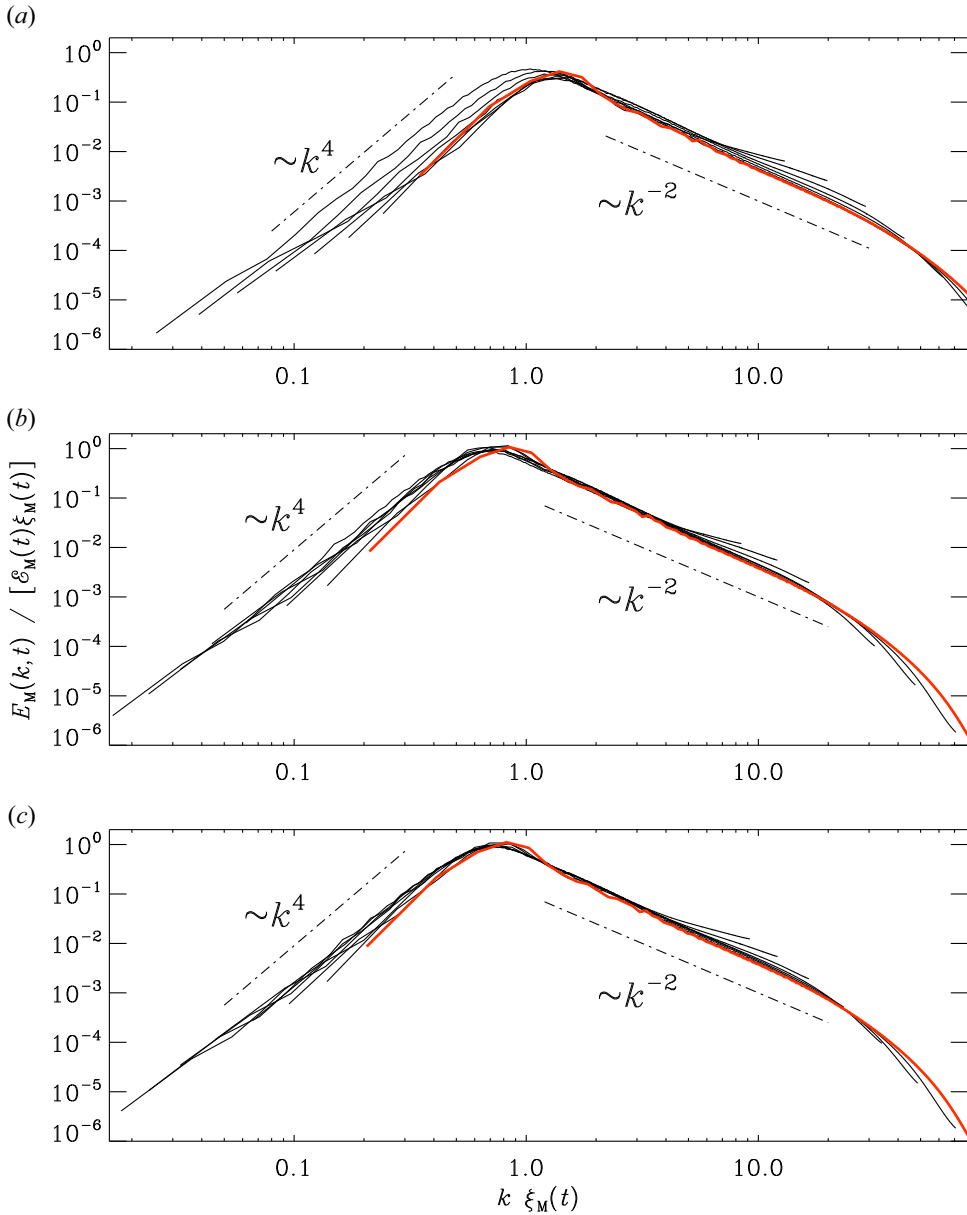


FIGURE 7. Magnetic energy spectra similar to figure 4, but the abscissa is scaled with $\xi_M(t)$ and the ordinate with $[\mathcal{E}_M(t)\xi_M(t)]^{-1}$, where (3.6) and (3.7) are used with $s = 1$ in (a) and with $s \rightarrow \infty$ in (b). In (c), the actual values of $\xi_M(t)$ and $\mathcal{E}_M(t)$ are used. The last time is shown as a thick red line.

that at the time of switchover, t_* , the real-space realizability condition (Biskamp 2003; Kahniashvili *et al.* 2010) is saturated, i.e. $2\xi_M(t_*)\mathcal{E}_M(t_*)/\rho_0 = I_M$. Next, inserting $\xi_M(t_*) = \xi_M(t_0) (t_*/t_0)^q$ and $\mathcal{E}_M(t_*) = \mathcal{E}_M(t_0) (t_*/t_0)^{-p}$, we find $2\xi_M(t_0)\mathcal{E}_M(t_0)/\rho_0 (t_*/t_0)^{-(p-q)} = I_M$, and therefore

$$t_* = t_0 \left[2\xi_M(t_0)\mathcal{E}_M(t_0)/I_M\rho_0 \right]^{1/(p-q)}. \tag{3.12}$$

For $p = 1$ and $q = 1/2$, we have $1/(p - q) = 2$ and recover the result of Tevzadze *et al.* (2012), while for $p = 10/9$ and $q = 4/9$, we have $1/(p - q) = 3/2$. Comparing with (3.11), we see that I_H enters with the same exponent $3/2$, and that the remainder can be identified with

$$I_H = [2\xi_M(t_0)\mathcal{E}_M(t_0)]^3 t_0^2. \quad (3.13)$$

This suggests that I_H is related to ξ_M and \mathcal{E}_M , but the problem is that t_0 is not straightforwardly related to the Alfvén time ξ_M/v_A , where $v_A^2 = 2\mathcal{E}_M/\rho_0$. Indeed, Brandenburg, Neronov & Vazza (2024) found that there is a pre-factor C_M that increases with increasing magnetic Reynolds number. Such a factor has been motivated based on magnetic reconnection arguments (Hosking & Schekochihin 2023a). Thus, inserting $t = C_M\xi_M/v_A$, we find

$$I_H = C_M^2 \xi_M^5 v_A^4. \quad (3.14)$$

The fact that C_M enters quadratically and approaches values in the range 20–50 for large magnetic Reynolds numbers explains why I_H strongly exceeds the naive estimate $\xi_M^5 v_A^4$. Interestingly, Zhou *et al.* (2022) found that part of the large excess over the naive estimate is related to non-Gaussianity. Another smaller part has to do with the spectral shape. Linking the value of C_M to non-Gaussianity of the magnetic field provides a new clue to the question of why there is a resistivity-dependent relation between decay and Alfvén times in hydromagnetic turbulence.

3.6. Can the switchover time be resistively limited?

We know that the decay time, $\tau(t) = (-d \ln \mathcal{E}_M/dt)^{-1} = t/p(t)$, can be regarded as resistively limited when relating it to the Alfvén time, $\tau_A = \xi_M/v_A$. In particular, as alluded to in § 3.5, it turns out that $\tau/\tau_A = C_M(Lu)$, which is a monotonically increasing function of Lu that saturates near Lu_* at $C_M^* \approx 50$ (Brandenburg *et al.* 2024). Such a relation was theoretically expected and has been associated with magnetic reconnection (Hosking & Schekochihin 2023a). However $C_M(Lu)$ was found to be independent of the value of the magnetic Prandtl number, which raised doubts about this interpretation.

The question now is whether the switchover time might also depend on the value of Lu . Differentiating (3.7) or (3.9), we see that the decay time depends on whether $t < t_*$ or $t > t_*$ and is equal to $9t/10$ or $3t/2$, respectively, but the switchover time itself is unaffected by resistivity effects. In other words, the decay time is always t/p , where the value of p depends on the time.

There is also the possibility that for $Lu < Lu_*$, the exponent p might depend on the order of the diffusion operator, i.e. on whether it is proportional to ∇^2 or some higher power; see Zhou *et al.* (2022) for details. However, this consideration only applies to the regime of low enough values of Lu and it would still not affect the actual value of t_* .

3.7. Hosking scaling at intermediate length scales

Hosking & Schekochihin (2021) presented arguments that for finite magnetic helicity, the Hosking scaling should only be obeyed at intermediate length scales. To check this, we now use the box-counting method as described by (2.7) to plot $\mathcal{I}_H(t, R)$ at different times t . The result is shown in figure 8 and resembles the sketch provided in figure 10 of Hosking & Schekochihin (2021). We do indeed see a short plateau where the Hosking scaling can be discerned for intermediate times. Furthermore, at later times, we see the expected R^3 scaling over the whole range of R .

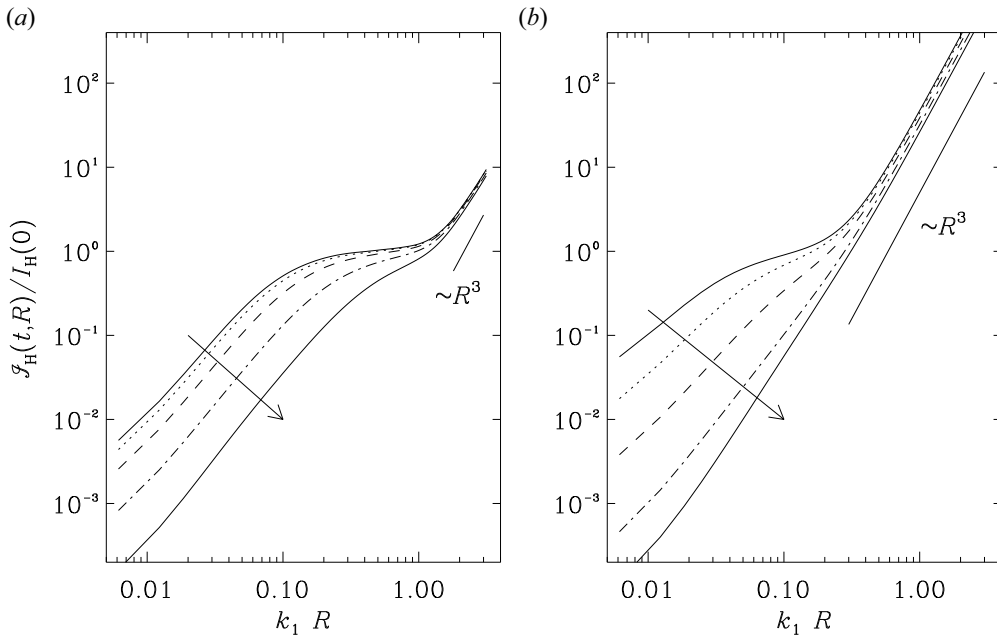


FIGURE 8. Box-counting result for $\mathcal{I}_H(R)$ for runs B and C in the left- and right-hand panels. Note the plateau for intermediate values of R at early times.

3.8. Comment on the case of a finite mean field

Our simulations presented above had zero mean field. It is well known that in the presence of a mean field across the entire domain, the magnetic helicity is no longer conserved (Berger 1997; Brandenburg & Matthaeus 2004); see Brandenburg *et al.* (2020) for corresponding decay simulations in the presence of a mean field. To check whether the Hosking integral could still be meaningful in such a case, we now present the time dependence of $I_H(t)$ for Run D with different magnetic field strength, where a mean field $\mathbf{B}_m = B_m \hat{x}$ is now imposed, so the magnetic field is given by $\mathbf{B} = \mathbf{B}_m + \nabla \times \mathbf{A}$. As before, we evaluate $I_H(t) = 2\pi^2 \text{Sp}(h)/k^2$ at $k = k_1$. The result is shown in figure 9 for four values of v_{Am} . We see that $I_H(t)$ is now decaying $\propto t^{-2}$, i.e. the Hosking integral is not conserved. Thus, with periodic boundary conditions, not only is I_M not conserved, but I_H is also not conserved.

3.9. Comment on the case with chiral fermions

As we have mentioned in the introduction, the Hosking integral also describes the decay of helical turbulence in the presence of chiral fermions if their chirality exactly balances the magnetic helicity. One may therefore ask whether a switchover to helical scaling could also occur in this case of the initial balance being not perfect. In Brandenburg *et al.* (2023a), two cases of imbalanced chirality were presented. In the case where the magnetic helicity exceeds the negative contribution to the chirality, a helical decay scaling $\propto t^{-2/3}$ of the magnetic energy was found, thus supporting our expectation. In the opposite case of an excess of fermion chirality, the time evolution of the magnetic energy was more complicated and no clear scaling suggestive of a helical decay was found.

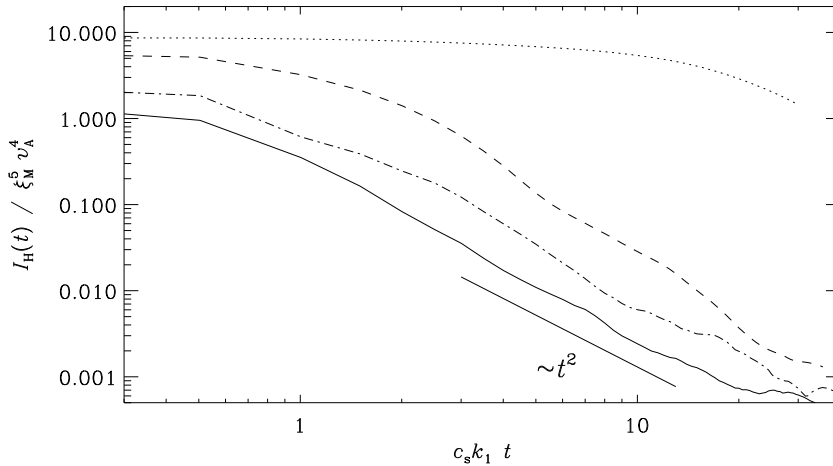


FIGURE 9. Time dependence of $\text{Sp}(h)$ for Run D (solid curve, $v_{\text{Am}}/c_s = 0.1$) and several cases with weaker mean field ($v_{\text{Am}}/c_s = 0.05$ for the dashed-dotted line, 0.02 for the dashed line and 0.01 for the dotted line).

4. Conclusions

The present work has shown that the decay laws for the combined case of two conserved quantities are best represented not simply by the sum of the individual laws, but that a good description of the numerical results is obtained by taking the maximum between the two individual decay laws. The switchover from one to the other decay law occurs earlier for $\xi_M(t)$ than for $\mathcal{E}_M(t)$. This behaviour is surprising, but confirmed by direct inspection of the two time traces in figures 5(b) and 5(d) and perhaps explained by changes in the shape of the magnetic energy spectrum during an otherwise almost perfectly self-similar decay.

Comparing with earlier work on the switchover from one to the other regime suggests that the ratio of the decay time to the Alfvén time enters in such a relation. This is remarkable, because in hydromagnetic turbulence the decay time is known to be longer than the Alfvén time by a resistivity-dependent factor of up to 50 (Brandenburg *et al.* 2024). This large factor might also explain why the value of the Hosking integral is always found to strongly exceed the naive estimate $\xi_M^5 v_A^4$. In other words, the reason why this simple formula underestimates the value of the Hosking integral might be the occurrence of the same resistivity-dependent factor that also occurs in the expression for the Alfvén time. However, as shown in Zhou *et al.* (2022), also other factors enter that involve the spectral shape. It would therefore be interesting to revisit this question.

As alluded to in the introduction, an obvious astrophysical application of our work is the decay of an initially bihelical magnetic field. Such situations are important in proto-neutron stars after the neutrino-driven convection ceases. Although this was actually our initial motivation, we have not analysed this case any further, because the most important aspect turned out to be the fact that the magnetic field has always fractional helicity in such cases, which we have now addressed in the present paper. A problem with the application to proto-neutron stars is of course the fact that in stars the magnetic field is inhomogeneous and the decay is initially not yet magnetically dominated; see Brandenburg *et al.* (2019) and Uchida *et al.* (2024). Another obvious application is to the decay of primordial magnetic fields during the radiation-dominated era of the early universe, which led to the aforementioned work by Tevzadze *et al.* (2012).

A more general question is that of a decay governed by two decay laws and whether there are other useful examples where the physics discussed in the present paper can be studied. As far as turbulence is concerned, one might think of the Saffman and Loitsyansky integrals, which represent the coefficients of the k^2 and k^4 terms in the Taylor expansion of the kinetic energy spectrum (see e.g. Davidson 2000). An initial k^4 spectrum (for a vanishing Saffman integral) might survive for some time, but neither of the two integrals is well conserved, and the Saffman integral might become important at later times when long-range interactions have occurred (Hosking & Schekochihin 2023b). This idea could also be applied to the magnetic case.

The case with an imposed magnetic field in a triply periodic domain is known to be peculiar. The mean magnetic helicity density of the remaining magnetic field (without the imposed one) is not conserved (Berger 1997). Although one can construct an additional quantity that takes the imposed field into account (Stribling, Matthaeus & Ghosh 1994), it turns out that it is not gauge-variant (Brandenburg & Matthaeus 2004). Our present work has shown that with an imposed mean magnetic field, also the Hosking integral is no longer conserved and tends to zero.

In summary, the present work has extended our knowledge about the Hosking integral, a remarkably useful quantity whose influence on many aspects of decaying hydromagnetic turbulence can be understood based on dimensional analysis. Numerical simulations are used to pinpoint the values of the coefficients. For several different systems, the set of these coefficients has been found to be similar, suggesting that their values might be fundamental quantities. But more work is required to establish this more firmly.

Acknowledgements

We thank I. Khaymovich and G. Vasil for inspiring discussions and useful comments on our work. We are also grateful to the three referees for their constructive remarks that have improved the presentation of our paper.

Editor Alex Schekochihin thanks the referees for their advice in evaluating this article.

Funding

This work was supported in part by the Swedish Research Council (Vetenskapsrådet, 2019-04234), the National Science Foundation under grant no. NSF AST-2307698 and NASA ATP Award 80NSSC22K0825. We acknowledge the inspiring atmosphere during the programme on the ‘Generation, evolution, and observations of cosmological magnetic fields’ at the Bernoulli Center in Lausanne. We acknowledge the allocation of computing resources provided by the Swedish National Allocations Committee at the Center for Parallel Computers at the Royal Institute of Technology in Stockholm and Linköping.

Declaration of interests

The authors report no conflict of interest.

Data availability statement

The data that support the findings of this study are openly available on Zenodo at <https://doi.org/10.5281/zenodo.14028931> (v2024.11.02) or, for easier access, at <http://norlx65.nordita.org/~brandenb/projects/Two-Conserved/>. All calculations have been performed with the PENCIL CODE (Pencil Code Collaboration *et al.* 2021); <https://doi.org/10.5281/zenodo.3961647>.

REFERENCES

- BANERJEE, R. & JEDAMZIK, K. 2004 Evolution of cosmic magnetic fields: from the very early universe, to recombination, to the present. *Phys. Rev. D* **70**, 123003.
- BERGER, M.A. 1997 Magnetic helicity in a periodic domain. *J. Geophys. Res.* **102** (A2), 2637–2644.
- BISKAMP, D. 2003 *Magnetohydrodynamic Turbulence*. Cambridge University Press.
- BISKAMP, D. & MÜLLER, W.-C. 1999 Decay laws for three-dimensional magnetohydrodynamic turbulence. *Phys. Rev. Lett.* **83** (11), 2195–2198.
- BRANDENBURG, A. 2020 Hall cascade with fractional magnetic helicity in neutron star crusts. *Astrophys. J.* **901** (1), 18.
- BRANDENBURG, A. 2023 Hosking integral in non-helical Hall cascade. *J. Plasma Phys.* **89** (1), 175890101.
- BRANDENBURG, A. & DAS, U. 2020 The time step constraint in radiation hydrodynamics. *Geophys. Astrophys. Fluid Dyn.* **114** (1–2), 162–195.
- BRANDENBURG, A., DURRER, R., HUANG, Y., KAHNIASHVILI, T., MANDAL, S. & MUKOHYAMA, S. 2020 Primordial magnetic helicity evolution with a homogeneous magnetic field from inflation. *Phys. Rev. D* **102** (2), 023536.
- BRANDENBURG, A., ENQVIST, K. & OLESEN, P. 1996 Large-scale magnetic fields from hydromagnetic turbulence in the very early universe. *Phys. Rev. D* **54** (2), 1291–1300.
- BRANDENBURG, A. & KAHNIASHVILI, T. 2017 Classes of hydrodynamic and magnetohydrodynamic turbulent decay. *Phys. Rev. Lett.* **118**, 055102.
- BRANDENBURG, A., KAHNIASHVILI, T., MANDAL, S., POL ROPER, A., TEVZADZE, A.G. & VACHASPATI, T. 2019 Dynamo effect in decaying helical turbulence. *Phys. Rev. Fluids* **4** (2), 024608.
- BRANDENBURG, A., KAHNIASHVILI, T. & TEVZADZE, A.G. 2015 Nonhelical inverse transfer of a decaying turbulent magnetic field. *Phys. Rev. Lett.* **114** (7), 075001.
- BRANDENBURG, A., KAMADA, K., MUKAIDA, K., SCHMITZ, K. & SCHOBER, J. 2023a Chiral magnetohydrodynamics with zero total chirality. *Phys. Rev. D* **108** (6), 063529.
- BRANDENBURG, A., KAMADA, K. & SCHOBER, J. 2023b Decay law of magnetic turbulence with helicity balanced by chiral fermions. *Phys. Rev. Res.* **5** (2), L022028.
- BRANDENBURG, A. & LARSSON, G. 2023 Turbulence with magnetic helicity that is absent on average. *Atmosphere* **14** (6), 932.
- BRANDENBURG, A. & MATTHAEUS, W.H. 2004 Magnetic helicity evolution in a periodic domain with imposed field. *Phys. Rev. E* **69** (5), 056407.
- BRANDENBURG, A., NERONOV, A. & VAZZA, F. 2024 Resistively controlled primordial magnetic turbulence decay. *Astron. Astrophys.* **687**, A186.
- BRANDENBURG, A., SHARMA, R. & VACHASPATI, T. 2023c Inverse cascading for initial magnetohydrodynamic turbulence spectra between Saffman and Batchelor. *J. Plasma Phys.* **89** (6), 905890606.
- BURROWS, A. & LATTIMER, J.M. 1986 The birth of neutron stars. *Astrophys. J.* **307**, 178.
- CHRISTENSSON, M., HINDMARSH, M. & BRANDENBURG, A. 2001 Inverse cascade in decaying three-dimensional magnetohydrodynamic turbulence. *Phys. Rev. E* **64**, 056405.
- DAVIDSON, P.A. 2000 Was Loitsyansky correct? A review of the arguments. *J. Turbul.* **1** (1), 6.
- EPSTEIN, R.I. 1979 Lepton-driven convection in supernovae. *Mon. Not. R. Astron. Soc.* **188**, 305–325.
- FRISCH, U., POUQUET, A., LEORAT, J. & MAZURE, A. 1975 Possibility of an inverse cascade of magnetic helicity in magnetohydrodynamic turbulence. *J. Fluid Mech.* **68**, 769–778.
- GOLDREICH, P. & REISENEGGER, A. 1992 Magnetic field decay in isolated neutron stars. *Astrophys. J.* **395**, 250.
- GUILLET, J., REBOUL-SALZE, A., RAYNAUD, R., BUGLI, M. & GALLET, B. 2022 MRI-driven dynamo at very high magnetic Prandtl numbers. *Mon. Not. R. Astron. Soc.* **516** (3), 4346–4353.
- HATORI, T. 1984 Kolmogorov-style argument for the decaying homogeneous MHD turbulence. *J. Phys. Soc. Japan* **53** (8), 2539.
- HOSKING, D.N. & SCHEKOCIHIN, A.A. 2021 Reconnection-controlled decay of magnetohydrodynamic turbulence and the role of invariants. *Phys. Rev. X* **11** (4), 041005.

- HOSKING, D.N. & SCHEKOCHIHIN, A.A. 2023a Cosmic-void observations reconciled with primordial magnetogenesis. *Nat. Commun.* **14**, 7523.
- HOSKING, D.N. & SCHEKOCHIHIN, A.A. 2023b Emergence of long-range correlations and thermal spectra in forced turbulence. *J. Fluid Mech.* **973**, A13.
- JI, H. 1999 Turbulent dynamos and magnetic helicity. *Phys. Rev. Lett.* **83** (16), 3198–3201.
- KAHNIASHVILI, T., BRANDENBURG, A., TEVZADZE, A.G. & RATRA, B. 2010 Numerical simulations of the decay of primordial magnetic turbulence. *Phys. Rev. D* **81** (12), 123002.
- KAHNIASHVILI, T., TEVZADZE, A.G., BRANDENBURG, A. & NERONOV, A. 2013 Evolution of primordial magnetic fields from phase transitions. *Phys. Rev. D* **87** (8), 083007.
- PARKER, E.N. 1955 Hydromagnetic dynamo models. *Astrophys. J.* **122**, 293–314.
- PENCIL CODE COLLABORATION, *et al.* 2021 The Pencil Code, a modular MPI code for partial differential equations and particles: multipurpose and multiuser-maintained. *J. Open Source Softw.* **6** (58), 2807.
- SCHEKOCHIHIN, A.A. 2022 MHD turbulence: a biased review. *J. Plasma Phys.* **88** (5), 155880501.
- STRIBLING, T., MATTHAEUS, W.H. & GHOSH, S. 1994 Nonlinear decay of magnetic helicity in magnetohydrodynamic turbulence with a mean magnetic field. *J. Geophys. Res.* **99** (A2), 2567–2576.
- TEVZADZE, A.G., KISSLINGER, L., BRANDENBURG, A. & KAHNIASHVILI, T. 2012 Magnetic fields from QCD phase transitions. *Astrophys. J.* **759**, 54.
- THOMPSON, C. & DUNCAN, R.C. 1993 Neutron star dynamos and the origins of pulsar magnetism. *Astrophys. J.* **408**, 194.
- UCHIDA, F., FUJIWARA, M., KAMADA, K. & YOKOYAMA, J. 2024 New comprehensive description of the scaling evolution of the cosmological magneto-hydrodynamic system. [arXiv:2405.06194](https://arxiv.org/abs/2405.06194).
- YOUSEF, T.A. & BRANDENBURG, A. 2003 Relaxation of writhe and twist of a bi-helical magnetic field. *Astron. Astrophys.* **407**, 7–12.
- ZHOU, H., SHARMA, R. & BRANDENBURG, A. 2022 Scaling of the Hosking integral in decaying magnetically dominated turbulence. *J. Plasma Phys.* **88** (6), 905880602.
- ZRAKE, J. 2014 Inverse cascade of nonhelical magnetic turbulence in a relativistic fluid. *Astrophys. J. Lett.* **794** (2), L26.